Journal of Controlled Release 351 (2022) 123–136

Contents lists available at ScienceDirect

Journal of Controlled Release

journal homepage: www.elsevier.com/locate/jconrel

Stable amorphous solid dispersion of flubendazole with high loading *via* electrospinning

Jana Becelaere [a,1], Elias Van Den Broeck [b,1], Ella Schoolaert [a], Valérie Vanhoorne [c], Joachim F.R. Van Guyse [d], Maarten Vergaelen [d], Sander Borgmans [b], Karolien Creemers [b], Veronique Van Speybroeck [b,*], Chris Vervaet [c,*], Richard Hoogenboom [d,*], Karen De Clerck [a,*]

[a] Ghent University, Center for Textile Science and Engineering, Faculty of Engineering and Architecture, Tech Lane Science Park 70A, B-9052 Ghent, Belgium
[b] Ghent University, Center for Molecular Modeling, Faculty of Engineering and Architecture, Tech Lane Science Park 46, B-9052 Ghent, Belgium
[c] Ghent University, Laboratory of Pharmaceutical Technology, Faculty of Pharmaceutical Sciences, Ottergemsesteenweg 460, B-9000 Ghent, Belgium
[d] Ghent University, Supramolecular Chemistry Group, Faculty of Sciences, Krijgslaan 281-S4, B-9000 Ghent, Belgium

ARTICLE INFO

Keywords:
Amorphous solid dispersions
Solvent electrospinning
Molecular dynamics
Computational chemistry
Poly(2-ethyl-2-oxazoline)
Flubendazole

ABSTRACT

In this work, an important step is taken towards the bioavailability improvement of poorly water-soluble drugs, such as flubendazole (Flu), posing a challenge in the current development of many novel oral-administrable therapeutics. Solvent electrospinning of a solution of the drug and poly (2-ethyl-2-oxazoline) (PEtOx) is demonstrated to be a viable strategy to produce stable nanofibrous amorphous solid dispersions (ASDs) with ultrahigh drug-loadings (up to 55 wt% Flu) and long-term stability (at least one year). Importantly, at such high drug loadings, the concentration of the polymer in the electrospinning solution has to be lowered below the concentration where it can be spun in absence of the drug as the interactions between the polymer and the drug result in increased solution viscosity. A combination of experimental analysis and molecular dynamics simulations revealed that this formulation strategy provides strong, dominant and highly stable hydrogen bonds between the polymer and the drug, which is crucial to obtain the high drug-loadings and to preserve the long-term amorphous character of the ASDs upon storage. *In vitro* drug release studies confirm the remarkable potential of this electrospinning formulation strategy by significantly increased drug solubility values and dissolution rates (respectively tripled and quadrupled compared to the crystalline drug), even after storing the formulation for one year.

1. Introduction

Approximately 40% of all marketed drugs and an estimated 90% of drugs in the pipeline can be classified as poorly water-soluble. [1,2] According to the Biopharmaceutical Classification System (BCS), these class II or IV active pharmaceutical ingredients (APIs) suffer from dissolution-related problems, which directly lowers their bioavailability. [3] Flubendazole (Flu) is a poorly water-soluble benzimidazole methylcarbamate anthelmintic, categorized as a BCS class IV compound. It is commonly used against gastrointestinal parasites in pigs and chickens. [4,5] Research has shown that Flu is highly effective as a microfilaricidal drug for *e.g.* lymphatic filariasis (river blindness) and onchocerciasis (elephantiasis), which are tropical diseases caused by filariae, *i.e.* parasitic roundworms. These human filarial infections affect over 150 million people in tropical areas. [4–11] Current oral formulations appear to be significantly less effective compared to parenterally administered doses due to the poor water-solubility of this highly crystalline drug. Unfortunately, severe reactions were reported around the injection site. [5,7,9,10,12] Therefore, a new formulation, preferably for oral administration, with enhanced Flu-bioavailability is required, which remains a major challenge. In fact, solubility-limited bioavailability is a significant general problem for poorly water-soluble drugs, since oral drug delivery is, and remains, the preferred route for drug administration. [13].

The formation of amorphous solid dispersions (ASDs) is one of the prominent routes to overcome poor water-solubility. [14] Chiou and

* Corresponding authors.
E-mail addresses: Veronique.VanSpeybroeck@UGent.be (V. Van Speybroeck), Chris.Vervaet@UGent.be (C. Vervaet), Richard.Hoogenboom@UGent.be (R. Hoogenboom), Karen.DeClerck@UGent.be (K. De Clerck).
[1] JB and EVDB contributed equally.

https://doi.org/10.1016/j.jconrel.2022.09.028
Received 6 April 2022; Received in revised form 30 August 2022; Accepted 13 September 2022

Riegelman gave a broad definition of the term solid dispersion entailing all types of solid dispersions. [14,15] However, the focus nowadays lies mostly on the completely amorphous solid dispersion of a hydrophobic API dispersed into an amorphous hydrophilic polymeric matrix to form a glass solution. [14,16] Vialpando et al. successfully obtained stable Flu-containing ASDs using polyvinylpyrrolidone (PVP) through spray drying and by using ordered mesoporous silica (OMS) with a maximum Flu-loading of 25 and 40 wt% respectively. [4] Nonetheless, several processing and stability issues remained. Indeed, while the amorphous state ensures a higher solubility and a faster dissolution rate due to its higher internal energy, it also provides an increased molecular mobility. This mobility is the cause of a lower overall physical stability, often resulting in recrystallization of the API in the formulation over time. [3,13,17,18] This physical instability can, however, be overcome by a rational selection of both the processing technique used to form the ASD and the polymer support, thereby ensuring a molecularly dispersed system which promotes API-polymer interactions and a high enough glass transition temperature to store the formulations in the glassy state. [13,17,19–21].

Solvent electrospinning is a polymer processing technique that produces membranes of nanofibers, with a diameter typically below 500 nm, upon application of electrostatic forces onto a viscous polymer solution. [22–24] It is hypothesized that the exceptionally fast solvent evaporation during electrospinning compared to other solvent processing techniques, *e.g.* solvent casting, [25] results in the random and higly dispersed kinetic entrapment of the API molecules within the rapidly dried polymer matrix. [17,26–28] The consequently reduced API-mobility is key for lowering the driving force for recrystallization, thus enhancing the physical stability of the ASD. [27,28] Moreover, the high porosity and large specific surface area of the nanofibrous nonwovens are beneficial for enhancing the dissolution rate of ASDs. [27,29–32] Combined with its easy implementation and up-scalability, electrospinning of API-polymer solutions is a promising ASD formulation technique. [26,29,33] Furthermore, the technique is very versatile, by altering the polymer or working coaxially, release profiles may be tuned to be sustained, thus broadening the possibilities tremendously. [34–38] Vigh et al. successfully applied electrospinning of PVP as a formulation technique for Flu, and explored its upscaling. Although promising, the obtained stable ASDs had a maximal Flu-loading of only 20 wt%. [39] To enhance patient compliance and comfort, it is preferred to reach as high as possible drug loadings, as this allows to reduce tablet size and the amount of excipient that is introduced into the body. However, limited research is put into drug loading capability, for both immediate release as for sustained release formulations. [35,40–44].

By selecting a proper polymeric carrier that induces specific API-polymer interactions such as Van der Waals forces or hydrogen bonds, the API-mobility can be reduced, hindering nucleation and recrystallization, and consequently enhancing biopharmaceutical properties such as shelf life-stability and solubility, even at higher API-loadings. [19,20,27] Good API-polymer miscibility is necessary [17,19,20] and the polymer should ideally maintain a supersaturated state upon dissolution, allowing a higher amount of API to be absorbed by the body. [19,20,45] Recent research demonstrated a better physical stability of ASDs of glipizide with poly(2-ethyl-2-oxazoline) (PEtOx) compared to ASDs with PVP. [46,47] Indeed, thanks to its amorphous nature combined with the presence of good hydrogen bond accepting groups, PEtOx is a good alternative to the generally applied amorphous hydrophilic polymers such as polyethylene glycol, polyvinyl alcohol and PVP (−derivatives). [17,27,56,48–55] PEtOx is a biocompatible, hydrophilic polymer comprised of tertiary amide units as part of the main chain and does not readily interact with proteins and cells, *i.e.* stealth behavior. [49–51,54,55,57] Several studies on PEtOx have shown zero cytotoxicity, high stability in the human body and no mucosal irritation or tissue damage, indicating that the polymer is safe to be used inside the body. [53,58,59] Based on limited research, it is already clear that PEtOx is a suitable and promising candidate as excipient for ASD formulations, enabling increased dissolution rates for the APIs it is being formulated with. [46,47,59].

In this work, the solubility enhancement (hence bioavailability, as soluble Flu can be taken up through the intestines) of Flu was investigated following formulation of highly drug-loaded PEtOx-based nanofibrous ASDs by electrospinning of Flu-PEtOx blends. Based on the chemical structures of Flu and PEtOx, it was expected that hydrogen bonding would occur between the two compounds, which is crucial for the physical stability of the ASDs. The Flu-PEtOx interactions were indeed revealed by infrared spectroscopy (ATR-FTIR) and additionally supported by an innovative multi-scale modeling approach, combining static density functional theory (DFT) calculations and molecular dynamics simulations using a new in-house derived polymer force field. For the latter, the complete electrospun Flu-PEtOx ASD structure was computationally mimicked resulting in the construction of realistic Flu-PEtOx ASD configurations, which were subjected to an extensive equilibration protocol. These models not only provided a tool to fundamentally understand the API-polymer interactions, but also to predict their influence on the final ASD behavior. Interestingly, the strong Flu-PEtOx hydrogen bonds allowed for ultra-high Flu-loadings (up to 55 wt%) in combination with decreased PEtOx concentrations in the spinning solutions, without affecting electrospinnability. The amorphous character of the ASDs was experimentally observed by modulated temperature differential scanning calorimetry (MDSC) and X-ray analysis, even after storage of one year. Theoretical self-diffusivity coefficients were calculated to investigate the Flu dynamics and underpin the long-term kinetic stability of the produced ASDs. Finally, the solubility and *in vitro* release of Flu was evaluated under sink conditions for various drug loadings. A comparison with ASDs formulated by solvent casting demonstrated the superior potential of electrospinning as a formulation technique that provides time-stable ASDs with high drug-loading and significanlty enhanced drug-solubility.

2. Experimental section/methods

2.1. Materials

Flu was purchased from UTAG (Almere, Netherlands). Defined PEtOx with an M_n of 50 kDa was synthesized as described below and according to previous literature. [60] 2-Phenyl-2-oxazoline (99%), tetrafluoroboric acid (48 wt% in H_2O) and methanol (>99.8%) were purchased from Sigma-Aldrich (Overijse, Belgium). Ninhydrin, barium oxide and ethyl acetate (acroseal® grade) were bought from Acros Organics (Geel, Belgium) and used as received. 2-Ethyl-2-oxazoline (Polymer Chemistry Innovations, Tuscon, USA) was purified by distillation over ninhydrin and bariumoxide. Formic acid (FA) (>98%) and hydrochloric acid (HCl) (37% in H_2O) were purchased from Sigma Aldrich (Overijse, Belgium) and used as such. All tests requiring an aqueous solution (pure H_2O or 0.1 M HCl solution) were carried out with distilled water of type III as considered in ISO Standard 3696.

2.2. Synthesis of poly(2-ethyl-2-oxazoline) with an M_n of 50 kDa

PEtOx with a molar mass of 50 kDa was synthesized according to a recently reported method. [60,61] Prior to polymerization, the solvent, ethyl acetate, and the monomer, 2-ethyl-2-oxazoline, were dried and purified. The initiator was a proton-initiated 2-phenyl-2-oxazoline tetrafluoroborate (HPheBF4) salt that was recrystallized from methanol. Before the reaction started, the initiator, HPheBF4 salt was gently melted under vacuum overnight to release any residual solvents. Using a VIGOR Sci-Lab SG 1200/750 Glovebox System, all reactants were added in the actual polymerization vessel containing the right amount of initiator needed for the polymerization. The reaction was aimed at a 70% conversion using a monomer-to-initiator ratio of 714:1 leading to an expected M_n of 50 kDa. Maintaining an inert, nucleophile free atmosphere, the reaction mixture was stirred at 60 °C in an oil bath for 5

days and 4 h until the desired M_n of 50 kDa was reached. Subsequently, the polymer mixture was terminated using an excess of a 1 M methanolic KOH solution. The polymer solution was purified by four consecutive steps of dilution with distilled water followed by rotary evaporation of the solvent under reduced pressure.

2.3. Polymer characterization

Size- exclusion chromatography was performed on an Agilent 1260-series HPLC system equipped with a 1260 online degasser, a 1260 ISO-pump, a 1260 automatic liquid sampler, a thermostatted column compartment set at 50 °C equipped with two PLgel 5 μm mixed-D columns (7.5 mm × 300 mm) and a precolumn in series, a 1260 diode array detector, and a 1260 refractive index (RI) detector. The used eluent was *N*,*N*-dimethyl acetamide containing 50 mM of LiCl at a flow rate of 0.5 mL/min. The spectra were analyzed using the Agilent Chemstation software with the GPC add on. Molar mass values and molar mass distribution, that is, dispersity (Đ), values were calculated against PMMA standards. A M_n of 62 kDa and a Đ of 1.3 was obtained (see Section S1, Fig. S1.1).

2.4. Electrospinning of solid dispersions

Electrospinning solutions were prepared by dissolving different amounts of Flu in FA. After full dissolution of Flu, the polymer was added and the solution was stirred until a homogeneous transparent solution was obtained. Mass concentrations are expressed by weight percentages defined for the polymer as the ratio of PEtOx mass and the sum of the PEtOx and solvent mass (Eq. (1)). For the amount of Flu in the system, the wt% is defined as the ratio of the mass of Flu to the sum of the Flu and PEtOx mass (Eq. (2)). The dynamic viscosity of the solutions was determined by an LVDV-II Brookfield viscometer (spindle S18, average error of 8%). All electrospinning experiments were carried out using a mononozzle set-up with an 18 gauge Terumo mixing needle without bevel. A stable Taylor cone was typically achieved at a flow rate of 0.1 mL·h^{-1}, a tip-to-collector distance of 20 cm, a voltage between 20 and 27 kV and a negative voltage at the collector of −5 kV. All electrospinning experiments were carried out under climatized conditions at 25 °C and 30% relative humidity in a Weisstechnik WEKK 10.50.1500 climate chamber. After electrospinning all samples were stored in a climatized lab at (23 ± 1)°C and a relative humidity of (25 ± 2)%.

$$wt\%_{PEtOx} = \frac{m_{PEtOx}}{m_{PEtOx} + m_{solvent}} \quad (1)$$

$$wt\%_{Flu} = \frac{m_{Flu}}{m_{Flu} + m_{PEtOx}} \quad (2)$$

2.5. Solvent casting

An entire range of ASDs with a Flu-loading ranging from 5 to 55 wt% was prepared *via* solvent casting (SC). In order to obtain homogeneous solutions a 15 wt% concentration of PEtOx was used. All solutions were prepared by dissolving different amounts of Flu in FA. After full dissolution of Flu the polymer was added and the solution was stirred. Once homogeneous solutions were obtained, the solutions were left overnight in a fumehood for FA evaporation. To ensure full solvent evaporation, the samples were stored in a desiccator and kept under vacuum for 1 week after which the samples were stored in a climatized lab at (23 ± 1)°C and a relative humidity of (25 ± 2)%.

2.6. Scanning electron microscopy

All produced nanofibrous membranes were analyzed on a Phenom XL Scanning Electron Microscope (SEM) at an accelerating voltage of 10 kV. Prior to analysis the samples were coated with gold using a sputter coater (LOT MSC1T). The nanofiber diameters were measured using FiberMetric software. The average diameters and their standard deviations were based on 500 measurements per sample.

2.7. Attenuated total reflectance Fourier transform infrared spectroscopy

Infrared (IR) spectra were recorded with a Nicolet™ IS50 Fourier Transform Infrared (FTIR) spectrometer equipped with an Attenuated Total Reflectance (ATR) accessory (diamond crystal) from Thermo Scientific. Samples were excited with light of wavenumbers ranging from 4000 up to 400 cm^{-1}. A resolution of 1 cm^{-1} and 32 scans for each sample was applied.

2.8. Thermogravimetric analysis

Thermogravimetric analysis (TGA) was performed on a Mettler-Toledo TGA/SDTA851e with Large Furnace and autosampler, using 70 μL alumina cubicles. Measurements were performed at 10 °C/min from 25 to 400 °C under nitrogen atmosphere. Evaluation was done *via* the STARe software, using blank corrections.

2.9. Temperature modulated differential scanning calorimetry

Temperature Modulated Differential Scanning Calorimetry (MDSC) was used to measure T_gs. A TA Instruments Q2000 equipped with a refrigerated cooling system (RCS90) was applied using nitrogen as purge gas (50 mL·min^{-1}). The instrument was calibrated using Tzero technology for standard Tzero aluminum pans using indium at the heating rate applied during the measurements. The heating rate was set at 2 °C·min^{-1} and samples of 2 ± 0.5 mg were used. A temperature modulation of ±0.3 °C every 60 s was selected. The samples were analyzed through an initial isothermal drying step at 100 °C for 30 min after which a heat-cool-heat cycle was set from 0 to 180 °C. The T_g was determined with TA TRIOS software. Experiments were performed in triplicate.

2.10. X-ray diffraction

All ASDs, both nanofibrous and solvent casted, were measured on an ARL™ X'TRA Powder Diffractometer of Thermo Scientific. The monochromatic X-rays are produced by a copper X-ray tube; Cu K-shell energy levels are equivalent to λ = 0.154056 nm. The diffraction patterns are recorded at an interval of 5 to 60° 2θ with a step size of 0.02° and a measuring time of 45 min. A Si (Li) solid state detector was used for data collection. To determine the sensitivity of the diffractometer towards the crystalline Flu, physical mixtures of PEtOx and Flu were prepared and measured accordingly. The nanofibrous ASDs were measured as such, while the SC samples were grinded to a powder.

2.11. UV–visible spectroscopy

UV–Vis spectra were recorded using a double beam Perkin-Elmer Lambda 900 UV–Vis spectrophotometer. Solutions were measured in transmission mode using quartz cells. The spectra were recorded from 250 nm to 400 nm with a data interval of 1 nm. Transmission was converted into absorbance (A) as these values provide a correlation with Flu concentration.

2.12. Determination of solubility

The solubility of Flu in its pure form and in the ASDs was determined in both H_2O and 0.1 M HCl using an ultrasonic bath. An excess amount of Flu, 50 ± 15 mg, or of the produced ASDs, containing 1 ± 0.05 mg Flu, was added to 10 mL H_2O (pH 6.75) or 0.1 M HCl (pH 1) solution. Mixtures were left in an 1510E Bransonic ultrasonic bath (42 kHz ± 6%) for three hours after which they rested vertically overnight prior to measurement. Samples were taken and filtered through a 0.45 μm PTFE

filter, diluted and consequently measured *via* UV–Vis spectroscopy. The Flu content was determined with respect to a calibration curve at 283 nm obtained prior to the measurements. Experiments were performed in triplicate.

2.13. *In vitro* dissolution tests under sink conditions

For both pure Flu and the produced SDs, *in vitro* dissolution tests were performed in 0.1 M HCl. After determination of the respective solubility, all measurements were performed under sink conditions, an equivalent of 5 mg of Flu was added to 1000 mL 0.1 M HCl dissolution medium (pH 1). The medium was stirred at a constant speed of 100 rpm throughout the measurements and samples were taken at different time intervals, *i.e.* 3, 5, 10, 15, 30, 45, 60, 90, 120, 150, 180, 240 and 300 min. Samples were filtered through a 0.45 μm PTFE filter, diluted and consequently measured *via* UV–Vis spectroscopy. The concentration of

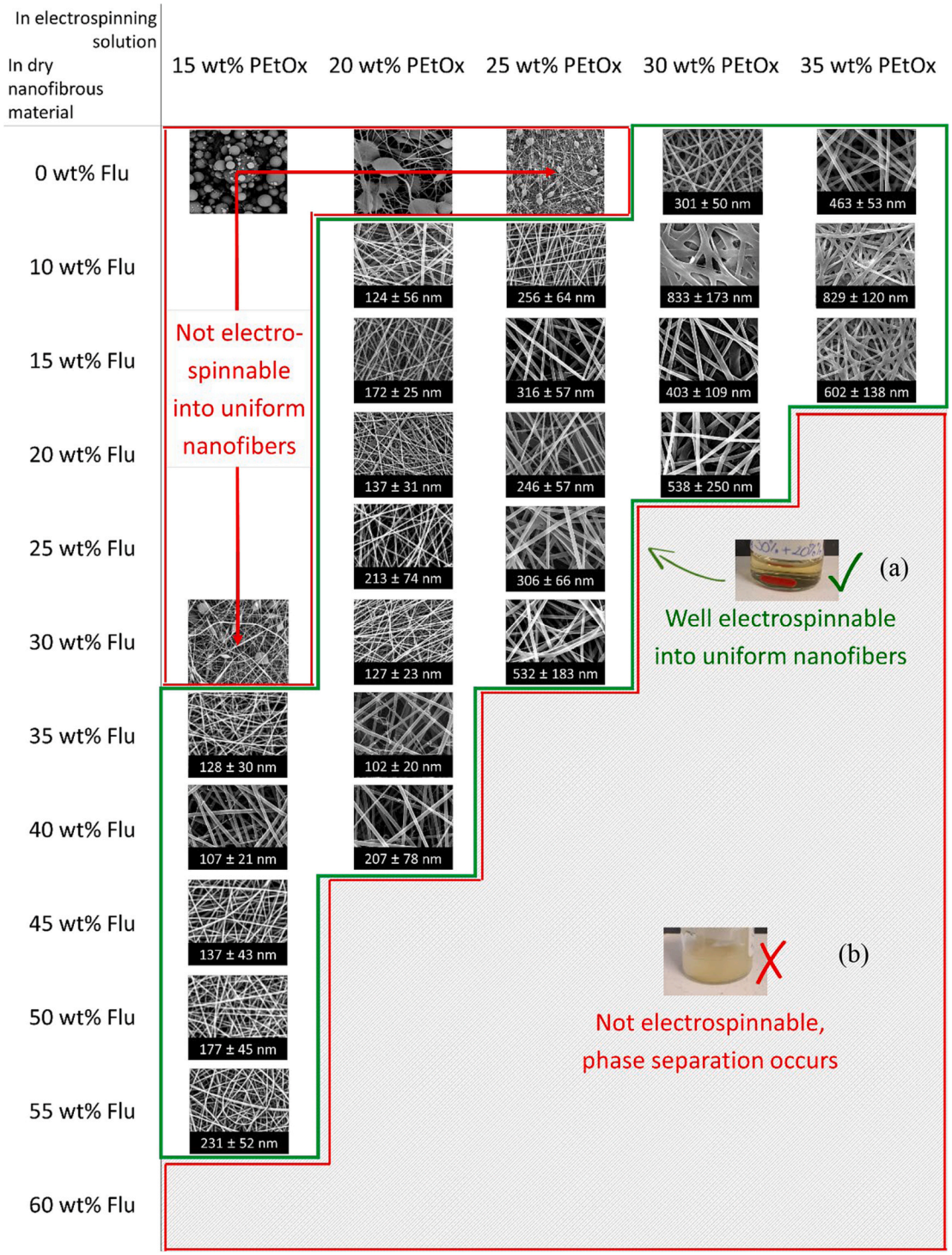

Fig. 1. Overview of all electrospinnable Flu-PEtOx blend solutions. All electrospinnable solutions were spun from a clear single-phase solution (a). When the amount of Flu exceeded its maximum solubility, a phase-separated system was obtained which was not electrospinnable (b). Clear evidence for Flu-PEtOx interactions can be seen for the 15 wt% PEtOx solutions, as a minimal concentration of Flu was required to obtain a stable electrospinning process. If the Flu concentration was below this limit (< 35 wt%), the viscosity of the solution was too low.

Flu present was determined with respect to a calibration curve at 283 nm obtained prior to the measurements. Experiments were performed in triplicate.

2.14. Computational methodology

As Flu-PEtOx interactions are crucial for the ASD stability, hence the solubility enhancement of Flu, the Flu-PEtOx interactions were also investigated by a multi-scale modeling approach to support and better understand the experimental observations. To this end, two types of simulations were performed. Firstly, a set of density functional theory (DFT) calculations was performed to assess whether Flu-PEtOx interactions are competitive with respect to Flu-Flu interactions (resembling the interactions present within a Flu-crystal). Secondly, large-scale atomistic force field-based simulations (>40,000 atoms) were performed on 50 wt% Flu-PEtOx ASDs, which were then compared to their pure compound counterparts regarding the nature and dynamics of occurring hydrogen bonds. Prior to these simulations, force fields were constructed for both PEtOx and Flu with the necessary validation performed in terms of density, T_g and XRD-pattern determination. For a full elaboration on the computational methodology, the reader is referred to section S2 of Supporting Information.

3. Results and discussion

3.1. Mapping the electrospinability of highly loaded Flu-PEtOx blends

Literature on electrospinning of PEtOx is limited, especially for well-defined (Đ < 1.5) PEtOx, and is mostly focused on waterborne electrospinning due to the water-solubility of the polymer. [32,62] On the other hand, to the best of our knowledge, the only available study on combined electrospinning of Flu with a polymer described the use of an ethanol-formic acid (FA) solvent system combined with PVP K90 as the polymer carrier. However, only 20 wt% Flu-loadings could be achieved due to the low solubility of Flu in this solvent system. [39] The low solubility of Flu in both water and ethanol inspired the selection of pure FA as a solvent system for electrospinning in the present work. The significant solubility of Flu in this solvent, *i.e.* 340 mg/mL, [4] was the main reason to opt for FA, as it might allow for higher Flu-loadings, resulting in a decrease in pill burden, beneficiating further downstream processing and patient compliance.

To the best of our knowledge, electrospinning of PEtOx from FA was not reported before, but is here shown to result in uniform nanofibers within a polymer concentration range of 30–35 wt% (Fig. 1, 0 wt% Flu). In general, an increasing fiber diameter was obtained with increasing polymer concentration, which is explained by the increase in viscosity, hence inter-chain interactions and entanglements. Subsequently, solutions with different polymer and Flu concentrations were prepared and electrospun, resulting in uniform beadless nanofibers when specific Flu-PEtOx ratios were used (Fig. 1). Within the PEtOx concentration range of 20–25 wt%, blends with a Flu-loading up to 30 wt% could be electrospun, but the available Flu-loading halved as the PEtOx concentration increased. At high polymer concentrations, *i.e.* 35 wt%, the Flu-loading was found to be limited to 15 wt%. If this limit was exceeded, inhomogeneous, phase-separated solutions were obtained, which could not be electrospun (Fig. 1, b), indicating that important interactions between the two components occur, leading to phase separation of Flu-PEtOx aggregates as both individual components were well-soluble in FA at the utilized concentrations. It is hypothesized that these interactions reduce the solubility through the formation of hydrogen-bonded coacervates. As a verification of this hypothesis, both components were solubilized in FA seperately and subsequently added together. Although the separate components were fully solubilized, the combination produced a phase-separated solution, indeed indicating the formation of the coacervate. As can be seen from Fig. 1 (a), however, the formation of the coacervates can be delayed if more solvent is present, *i.e.* the PEtOx concentration is reduced. In this way, higher Flu-loadings can be achieved. Interestingly, the occurrence of the Flu-PEtOx interactions allows for the fabrication of uniform nanofibers at PEtOx-concentrations (15–25 wt%), which is out of the electrospinning range of pure PEtOx in FA, as this leads to electrospraying in the absence of Flu due to a too low solution viscosity. A minimum Flu-loading of 35 wt% is even required for electrospinning of nanofibers if only 15 wt% of PEtOx is present in the spinning solution to ensure enough inter-chain interactions and entanglements, thus solution viscosity, for uniform nanofiber formation (Table S1.1). As such, ultra-high Flu-loadings up to 55 wt% could be achieved by lowering the PEtOx concentration without affecting electrospinnability. To the best of our knowledge, it is the first time that it is demonstrated that nanofibers with increased drug-loading can be achieved by reducing the polymer concentration below its individual electrospinnability window.

This result indicates that the strong Flu-PEtOx interactions determine the electrospinnability window of the blend and that this window is shifted towards higher Flu-loadings to provide sufficient interaction with lower PEtOx concentrations. In other words, the Flu-PEtOx interactions allow, within a specific range, to increase the drug-loading simply by reducing the polymer concentration. Thus, these strong API-polymer interactions are not only necessary to achieve physical stability of the ASD, but they are also key to achieve high drug-loadings through electrospinning, and it is, therefore, crucial to investigate and understand the possible interactions of the intended API-polymer system.

3.2. Experimental and computational analysis of Flu-PEtOx interactions

The PEtOx-Flu interactions observed during electrospinning are crucial for the success of the produced formulation. Indeed, certain API-polymer interactions are required to enhance the physical stability of the ASDs. [20,63] ATR-FTIR spectroscopy was first performed to investigate these interactions. [64] As shown in Fig. 2 (inset b) the spectrum of a Flu-PEtOx ASD significantly differs from both the spectra of the pure components, suggesting intermolecular interactions. PEtOx has two hydrogen bond acceptors (Fig. 2, inset a, highlighted in red) and no hydrogen bond donors, while Flu has two hydrogen bond donors (Fig. 2, inset a, highlighted in blue). Hydrogen bonding between both components is hence expected to occur and confirmed by the three spectral regions highlighted in Fig. 2. The distinctive secondary amine N—H stretch of Flu at 3306 cm^{-1} has disappeared in the ASDs, which is consistent with the appearance of hydrogen bridges, shown in Fig. 2 (inset c). [65] Furthermore, the characteristic PEtOx peak representing the C═O stretch of the carbonyl group (Fig. 2, inset d) is shifted to higher wavenumbers, confirming the presence of interactions with Flu. Additionally, this peak decreases in intensity with increasing Flu-loading, which is explained by a lower PEtOx fraction present in the ASDs. Lastly, Fig. 2 (inset e) shows the Flu peak shift for the characteristic C—N stretch of the secondary amine, further indicating the presence of hydrogen bridges. The most probable hydrogen bonding interactions between Flu and PEtOx are illustrated in Fig. 2 (inset a) and were theoretically supported by DFT calculations and radial distribution functions (rdfs) extracted from molecular dynamics simulations (see section S2.1). It should be noted that for ease of interpretation and computational cost, the assumption of no residual solvent in the ASD was made.

DFT calculations were first performed to assess whether Flu-PEtOx interactions are occurring and if they are competitive with respect to Flu-Flu interactions (resembling the interactions present within a crystal). For this, the most stable configurations of the polymer, the Flu-Flu complex and the Flu-PEtOx complex were determined and the calculated negative complexation energies indicated that the formation of hydrogen bonds is of major importance for the stability of these complexes and that interactions between PEtOx and Flu are favorable (Fig. 2, inset f, and Fig. S2.1). However, based on the complexation energies, it

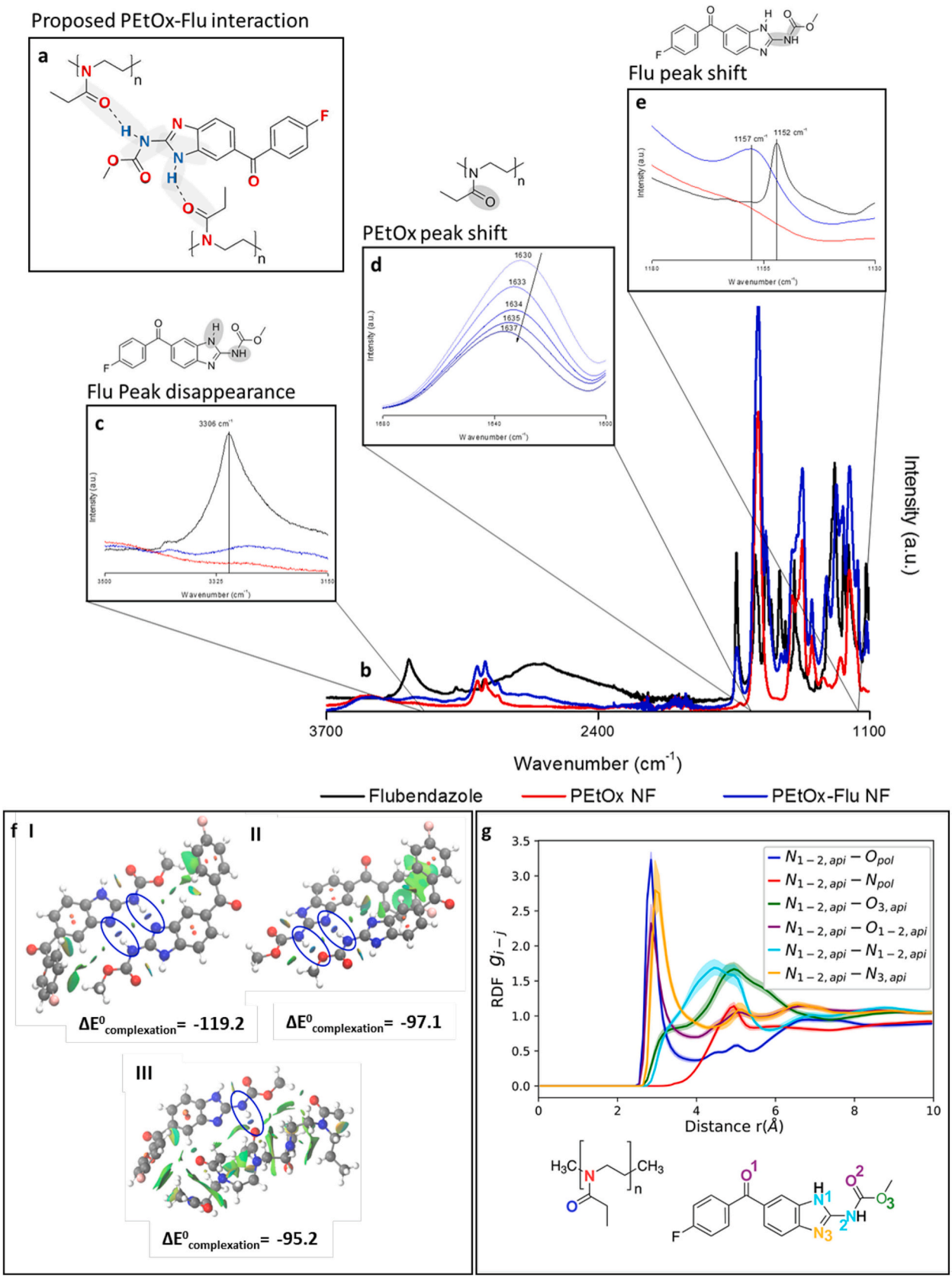

(caption on next page)

Fig. 2. Results of ATR-FT-IR spectroscopy. (a) The proposed interaction between PEtOx and Flu. (b) ATR-FTIR spectrum of Flu (black), PEtOx nanofibers (red) and the prepared Flu-PEtOx ASDs (blue). Insets (c), (d) and (e) highlight areas in the ATR-FTIR spectrum where Flu-PEtOx interaction is noticeable. (c) The inherent Flu peak at 3306 cm^{-1}, N—H stretch of the secondary amine, has disappeared for all ASDs. (d) A peak shift of the distinctive C═O stretch of PEtOx is observed. This peak shift is related to the Flu-loading, the peak shifts further to the left when more Flu is present and due to a decrease in PEtOx present in the material the peak also decreases in intensity. (darker blue equals a higher Flu-loading). (e) Irrespective of the Flu-loading, a peak shift is noticed for the distinctive C—N stretch of the secondary amine of Flu when formulated as an ASD. (f) Overview of the most stable configurations based on DFT calculations: I) Most stable Flu-Flu complex with two hydrogen bonds (N−*H*−N); II) Flu-Flu complex with two hydrogen bonds (N-H-N and N-H-O(ether)) and π-π interactions; III) Flu-PEtOx complex with one hydrogen bond (N-H-O(carbonyl). ΔG and ΔE (complexation energies) are given in units of kJ·mol-1 and calculated at the ωB97XD-6-311 + g(d,p) level of theory (1 atm, 297.15 K) with inclusion of BSSE-corrections when appropriate; green surfaces represent weak van der Waals interactions, red surfaces represent repulsive interactions and blue attractive/stabilizing interactions (displayed using the NCI-plot tool, see section S2.2). Hydrogen bonds are highlighted with blue ellipses. (g) Radial distribution functions (with 95% confidence intervals) for the different highlighted atom pairs in the ASDs. (For interpretation of the references to colour in this figure legend, the reader is referred to the web version of this article.)

is also expected that, with increasing concentration of Flu-molecules, Flu-Flu complexation will start dominating, eventually resulting in phase separation. Other Flu-Flu complexation energies were within the same range as Flu-PEtOx complexation energies, indicating that the hydrogen bond (NH-O) strength is similar, hence competition for the hydrogen bond donor sites is present.

Subsequently, to simulate interactions present in realistic systems allowing to study the PEtOx-Flu ASDs in detail, large-scale force field calculations were performed to mimic the electrospun Flu-PEtOx ASDs as completely as possible (Fig. 3 and section S2.2). Table 1 provides strong evidence that the developed computational procedure (Figs. S2.2 and S2.3) can consistently construct ASDs, showing that the calculated densities, T_gs and X-ray diffractograms were in good agreement to the experimental values (section Evaluation of the amorphous structure and compound miscibility and Figs. S2.4, S2.5 and S2.6). Additionally, it shows that the simulated systems perform well to describe the real Flu-PEtOx ASDs, allowing to not only study and underpin in detail the present interactions in known systems, but also to predict the ASD characteristics and behavior under different experimental conditions.

Taking into account the necessity of the aging step within the procedure (Fig. 3 and section S2.2.8, Fig. S2.7), production simulations were subsequently performed at the experimental conditions (section S2.2.9, Figs. S2.8 and S2.9) which were used to analyze the various pairwise interactions present in the ASDs by means of rdfs (Fig. 2, inset g) and visual inspection (Fig. 3 and Fig. S2.9). Additionally, a hydrogen bonding analysis is performed to assess the amount and dynamics of the different hydrogen bonding pairs (*vide infra* and section S2.2.10). [68].

Fig. 2 (inset g) shows the rdfs of various possible hydrogen bonding pairs within the simulated 50 wt% Flu-PEtOx ASDs. Hydrogen bonds were, indeed, observed within the simulated ASDs and the patterns

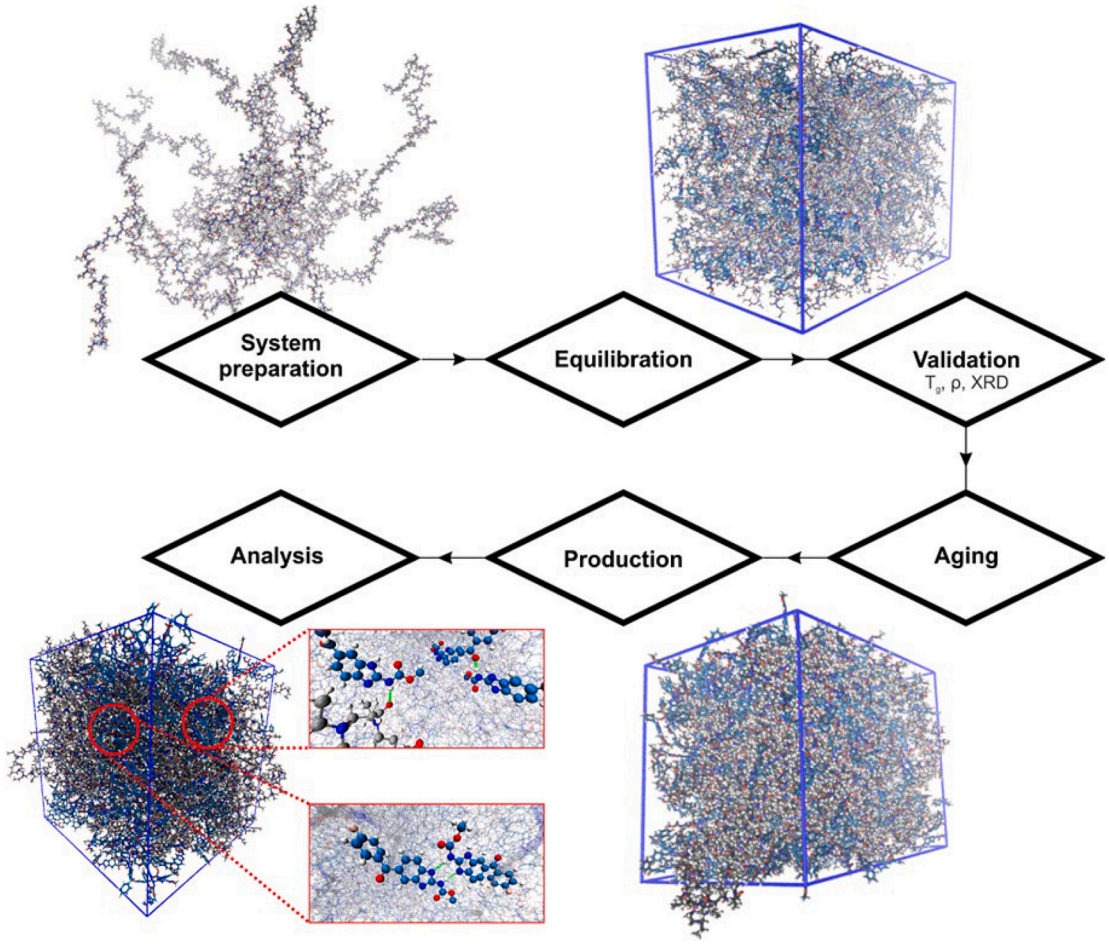

Fig. 3. Workflow of the computational procedure to simulate and investigate realistic electrospun ASDs, highlighting each step of the computational protocol. Structures illustrate the change in packing during the equilibration protocol. Upon visual inspection of the generated structure, the present interactions can be clearly observed (as highlighted under 'Analysis'). A more elaborate representation of the applied workflow is shown in section S2.2.4.

Table 1
Density and T_g validation results obtained from the equilibrated and aged structures.

# Flu	$\rho_{equilibration}$ [g·mL^{-1}][a]	ρ_{aged} [g·mL^{-1}]		T_g [K]			
		MD[b]	Exp.	MD[b]	Δ	Exp.[c]	Δ
0 (0 wt%)	1.1226 ± 0.0018	1.1326 ± 0.0058	1.14 [67]	348 ± 10	22	335 ± 0.6	25
476 (50 wt %)	1.2095 ± 0.0009	1.2180 ± 0.0053	–	370 ± 11		360 ± 0.8	
10 (5 mg·mL^{-1})	1.01468 ± 0.00004	–	–	–			
250 (5x5x5 crystal)	1.462	–	1.444	–			

$\rho_{equilibration}$ represents the density of the equilibrated system (before aging), ρ_{aged} represents the density of the system after the physical aging step of the protocol. T_g are the glass transition temperatures of the equilibrated structures obtained through the protocol discussed in section S.2.2.6, Δ-values represent the difference between the T_g for the pure polymeric amorphous system and the ASD containing 50 wt% Flu. #Flu = 0 wt%, 50 wt%, 5 mg·mL^{-1} and 5x5x5 crystal represent the pure polymeric system, the ASD containing 50 wt% Flu, an aqueous solution of Flu at a concentration of 5 mg·mL^{-1} and a Flu 5x5x5 crystal configuration, respectively.

[a] 95%-Confidence intervals are constructed based on the results of ten different input structures which are subsequently bootstrapped with replacement.

[b] 95%-Confidence intervals are constructed based standard uncertainty value for the results of three different input structures for which a coverage factor of 4.30 (t-distribution) is used, assuming a gaussian-distributed observable.

[c] Standard deviation given after three measurements.

observed throughout the different rdfs highlight that mainly N_3 (Fig. 2, inset g, orange curves) and the carbonyl oxygen atoms Fig. 2, inset g, blue and purple curves) were participating as hydrogen bond acceptors, both in PEtOx-Flu and Flu-Flu hydrogen bonding. Furthermore, from the confidence intervals, it is clear that these persisted within the different input structures used in the study. Visual inspection of the simulated PEtOx-Flu ASD configuration further confirms these results, as the various interactions in the ASD could be clearly observed upon zooming in (highlighted in Fig. 3 and Fig. S2.9). Hence, it can be concluded that mainly the carbonyl oxygen groups of the PEtOx participate in the hydrogen bonding interactions between PEtOx and Flu, which supports the experimental ATR-FTIR analysis.

In order to study which hydrogen bonding pairs are dominating (*i.e.* Flu-Flu or Flu-PEtOx) in the simulated ASD with 50 wt% Flu, and whether a difference exists between the trends observed for the ASDs and the crystal structure, the total number of hydrogen bonds present within the production runs was determined (Table 2 and Fig. S2.10). Additionally, to assess the persistency (and hence the dynamics) of the various hydrogen bonds, continuous hydrogen bond lifetimes were determined (Table 2 and Fig. S2.11). [68] These represent the average time that a hydrogen bonding pair remains intact and, therefore, provides information on the average life time of a hydrogen bond (once a bond is broken it will be considered broken from that moment on).

Simulated 50 wt% Flu-PEtOx ASDs show a significant increase in the total number of occupied hydrogen bond donor sites with respect to crystalline Flu. As was already indicated by DFT calculations, a competition occurs between PEtOx and Flu for donor sites. According to the simulations (Table 2), this competition is, at least for this weight percentage, dominated by PEtOx, *i.e.* 16.7% compared to 10.4% of the sites for Flu, which is favorable for the experimental electrospinability of the system as well as the physical stability of the ASD. Additionally, τ_c indicates that for Flu-PEtOx the bonds are stronger and are preserved during relatively long periods of time within the material, *i.e.* once a hydrogen bond was formed it remained intact for 2.12 ns while for Flu-

Table 2
Fraction of occupied hydrogen bond donors and continuous hydrogen bond lifetimes within the crystal and the ASD for the different constituents within the materials.

System	Hydrogen bond occupied by	Fraction occupied hydrogen bonds[a]	Continuous hydrogen bond lifetime τ_c [ns][b]
50 wt% ASD	Total	0.271 ± 0.017	1.76 ± 0.420
	Flu	0.104 ± 0.018	1.25 ± 0.348
	PEtOx	0.167 ± 0.006	2.12 ± 0.464
Flu-crystal	Flu	0.145 ± 0.005	1.06 ± 0.169

For comparability, the results were normalized by the total amount of available hydrogen donors within the system (*i.e.* two times the number of Flu-molecules present within the system). For a graphical overview of the occupied hydrogen bonds during the production runs and the correlation functions used to derive the lifetimes, the reader is referred to Figs. S2.10 and S2.11.

[a] 95%-Confidence intervals are constructed based on the results of ten different input structures which are subsequently bootstrapped with replacement.

[b] 95%-Confidence intervals are constructed based standard uncertainty value for the results of three different input structures for which a coverage factor of 2.26 (t-distribution) is used, assuming a gaussian-distributed observable.

Flu this was 'only' 1.25 ns. Furthermore, a significant increase was observed for the lifetimes in the Flu-PEtOx ASD (1.8 ns) with respect to the Flu-crystal (1.0 ns) when accounting for all hydrogen bonds present (Table 2, 'Total'). Both for the Flu-crystal and the Flu-PEtOx ASDs these lifetimes indicate that the formed hydrogen bonds are very stable within the material and far from dynamic (*e.g.* with respect to results reported by Gower et al. [68]), indicating that the formed material could be stabilized by these type of interactions. A result, which is, indeed, experimentally observed by the amorphous nature of the ASDs and its long term stability.

3.3. Amorphous nature of the Flu-PEtOx ASDs and its long term stability

3.3.1. Evaluation of the amorphous structure and compound miscibility

To study the amorphous nature of Flu in the ASDs, XRD and MDSC measurements were performed. Based on the XRD patterns of Flu-PEtOx physical mixtures with varying Flu-loadings, a distinctive Bragg peak at 6.5° could be distinguished when at least 3 wt% crystalline Flu was present (Fig. 4, a). By further increasing the Flu-loading, other Flu-related Bragg peaks started to appear. In contrast, no Bragg peaks could be observed in the XRD patterns of any of the nanofibrous Flu-PEtOx ASDs, clearly displaying a fully amorphous nature, [69] even up to a Flu-loading of 55 wt% (Fig. 4, b). It can thus be concluded that all electrospun ASDs contained <3 wt% detectable crystalline Flu, a result which is crucial for the solubility enhancement of Flu. Electrospinning of Flu-PEtOx blends, therefore, allows to fabricate fully amorphous ASDs containing Flu-loadings as high as 55 wt%, which is unprecedented. The amorphous nature of the electrospun Flu-PEtOx ASDs was additionally predicted by XRD-patterns generated by the computational model (Fig. S2.6).

MDSC was additionally applied to assess the miscibility and single-phase character of the ASDs, which relates to the Flu-PEtOx interactions and, consequently, the ASDs physical stability. [4] Note that MDSC could not be used to assess crystallinity as the melting peak of Flu (238 °C) [4] is located above the degradation temperature of Flu (225 °C, Fig. S1.2). The MDSC thermograms of the nanofibrous ASDs (Fig. 4, c) revealed a homogeneous system, similar to what was expected from the force field calculations. Moreover, all T_gs were situated in between the T_g of pure Flu (156 °C) [4] and PEtOx (61.5 °C) (Table S1.2), suggesting a good miscibility between both components. The T_gs were analyzed using the Fox (Eq. (3)) and Gordon-Taylor (Eq. (4)) models.

$$\frac{1}{T_g} = \frac{w_1}{T_{g1}} + \frac{w_2}{T_{g2}} \tag{3}$$

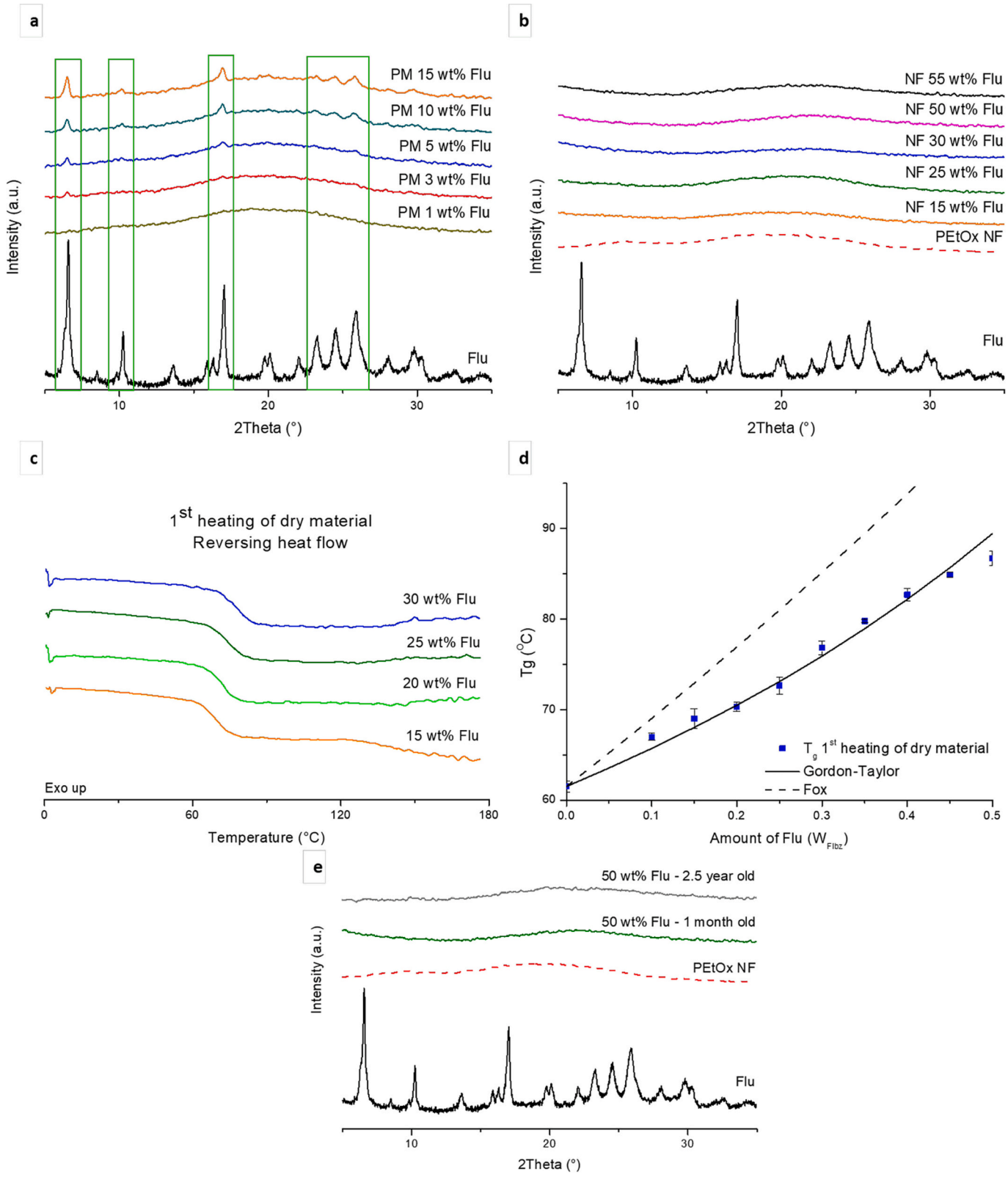

Fig. 4. XRD patterns of physical Flu-PEtOx mixtures with an increasing amount of Flu show Bragg peaks from 3 wt% Flu-loading onwards (a, Flu-related Bragg peaks are highlighted in the green boxes), while Flu-PEtOx ASDs show no Bragg peaks up to Flu-loadings of 55 wt%, confirming the amorphous nature of the ASDs (b). (c) MDSC analysis of the prepared Flu-PEtOx ASDs shows a clear single T_g is observed in between the Tg of the pure components (156 °C for Flu [4] and 61.5 °C for PEtOx NF). (d) T_g analysis of Flu-PEtOx ASDs. Values were compared to the theoretical values predicted by Fox equation and fitted against the Gordon-Taylor equation with a k value of 0.42. (e) The XRD pattern shows no sign of Bragg peaks related to crystalline Flu, indicating a fully amorphous ASD even after two and a half years. (For interpretation of the references to colour in this figure legend, the reader is referred to the web version of this article.)

$$T_g = \frac{w_1 T_{g1} + k w_2 T_{g2}}{w_1 + k w_2} \quad (4)$$

with T_g being the glass transition temperature of the ASD, wi and T_{gi} the respective weight fraction and T_g of the pure components. The subscript 2 refers to the component with the highest T_g, which is Flu in this case. [70] The Fox model assumes homogeneous mixing and no specific interactions between both components. [71] The Gordon-Taylor model, on the other hand, takes into account the specific coefficients of expansion in the rubbery and glassy state of the pure components based on the constant k (Eq. (5)). [72]

$$k = \frac{\Delta\alpha_2 \rho_1}{\Delta\alpha_1 \rho_2} \quad (5)$$

where $\Delta\alpha_i$ and ρ_i are the change in cubic expansion coefficient and the density of the components at the T_g, respectively. [73] The experimentally obtained T_gs correspond well with the theoretically predicted values using the Gordon-Taylor model with a fitting parameter k of 0.42 (Fig. 4, d, and Table S1.2). The Gordon-Taylor model also assumes ideal mixing, hence complete miscibility, of both components. [70] Therefore, the obtained fit confirms the miscibility between Flu and PEtOx, a result that is crucial for the physical stability of the ASDs, as intimately mixed systems are more likely to resist crystallization. [43,63,74,75] Moreover, it experimentally confirms the results obtained by the performed simulations.

3.3.2. Flu mobility and long term ASD stability

For real-life applications, the long term stability of the ASDs is a crucial factor. Molecular dynamic simulations (see section Experimental and computational analysis of Flu-PEtOx interactions) indicated that the obtained ASDs could be significantly stabilized due to the presence of the strong and stable Flu-PEtOx hydrogen bonds. This statement was verified by evaluating the stability of an electrospun Flu-PEtOx ASD with a Flu-loading of 50 wt% that was stored at 23 °C and 25% relative humidity for two and a half years. Fig. 4 (e) shows the XRD spectrum of this stored sample, still revealing a fully amorphous material, which indicated the long term physical stability of electrospun nanofibrous Flu-PEtOx ASDs. To further understand the experimentally observed stability of the electrospun ASDs, the mobility of Flu within the ASDs was investigated by computation of self-diffusivity coefficients with respect to pure Flu (crystal) and Flu dissolved in water (5 mg/mL, section S2.2.11, Fig. S2.12). As the self-diffusivity coefficients of a 50 wt% Flu-PEtOx ASD (5.459 ± 1.183·10–8 $cm^2 \cdot s^{-1}$) and a Flu-crystal (5.456 ± 3.2·10–8 $cm^2 \cdot s^{-1}$) were very similar, it could be concluded that the Flu-molecules are effectively trapped within the ASDs, as is the case for Flu-molecules within a Flu-crystal. To put this into perspective, the self-diffusivity of Flu-molecules in an aqueous environment was two orders of magnitude higher (2.679 ± 1.403·10–6 $cm^2 \cdot s^{-1}$), highlighting the relatively fast dynamics of the molecules in biological environments. The observed trend nicely illustrates how the polymer matrix can serve as a kinetic trap for the Flu-molecules in case the ASD is prepared by electrospinning, thereby inducing long-term stability, which is perfectly in line with the long-term stability experiments and hydrogen bond lifetimes presented above.

3.3.3. Solubility and release rate enhancement through in vitro sink drug delivery testing

APIs belonging to the BCS class II and IV, such as Flu, suffer from a low bioavailability due to their limited solubility and, therefore, low dissolution rate. The effect of electrospinning Flu-PEtOx ASDs as a formulation strategy to increase aqueous solubility and dissolution rates was, therefore, analyzed by *in vitro* Flu release tests. To determine the sink conditions that were used for the *in vitro* release testing, the equilibrium solubility of Flu and several ASDs was determined in both pH 1 and pH 6.75 media (Table S1.3). The positive effect of the amorphous structure on the solubility is already evident, as the equilibrium solubility of Flu is 2.6 times higher (pH 1) when formulated as an ASD compared to its crystalline counterpart. Note that the equilibrium solubility of Flu is 32 times higher in acidic medium compared to neutral medium, which can be attributed to the protonation of the benzimidazole group at low pH. [76,77] *In vitro* sink dissolution tests were subsequently performed to assess dissolution rates (Table S1.4). A substantial difference between Flu in its crystalline form and within the ASD formulations was observed. While after five hours only 37% of crystalline Flu was dissolved (Fig. S1.3), all ASDs reached almost full Flu release during the first hour already (Fig. 5, a).

The initial dissolution rates (Table S1.4), clearly demonstrate that formulating Flu in a PEtOx-based ASD nanofibers *via* electrospinning increased the dissolution rate by 4.3 times on average. No significant effect of the Flu-loading was noticed in the dissolution profiles of the ASDs. Fig. 5 (b) additionally shows the sink dissolution profile of an 25 wt% ASD that was stored for one year compared to crystalline Flu and an ASD stored for one week. Remarkably, no significant differences were observed, revealing the same dissolution profile after one week and one year, with respective dissolution rates of 0.31 ± 0.03 $\mu g \cdot mL^{-1} \cdot min^{-1}$ and 0.30 ± 0.08 $\mu g \cdot mL^{-1} \cdot min^{-1}$ during the first ten minutes (Table S1.5). A similarity factor f_2, as described by Shah et al., [78] of 60.5 was obtained, meaning that the average difference between the two dissolution profiles is only around 6%. These results indicate the potential of electrospinning and the ability of PEtOx as an excipient to stabilize the amorphous form of Flu and inhibit recrystallization, both upon dissolution and over time.

3.3.4. Solvent electrospinning vs. solvent casting

The ability of electrospinning to obtain fully amorphous ASDs is hypothesized to be a consequence of the extremely rapid solvent evaporation throughout the electrospinning process, which leaves very limited time for the system to reorganize and phase separate (due to Flu crystallization) before it is frozen into place. [27,79] As a validation of this hypothesis, another solvent method for the creation of Flu-PEtOx ASDs was evaluated, *i.e.* solvent casting (SC). Identical Flu-PEtOx solutions as those used for electrospinning were prepared and the solution was left to evaporate at ambient temperature. This means that a considerable timespan was provided for full solvent evaporation, in which there was molecular mobility of Flu. Given that there is more time for rearrangement of Flu, it was expected that recrystallization was more likely to occur, which was indeed confirmed by XRD analysis. From 15 wt% Flu-loadings onwards, the SC ASDs were no longer fully amorphous, as the SC ASDs with 20 and 25 wt% Flu-loadings clearly showed a small Bragg peak at 6.5° (Fig. 6). SC could, therefore, only guarantee a fully amorphous ASD material at low Flu-loadings, which is in strong contrast with the electrospun nanofibrous ASDs enabling Flu-loadings up to 55 wt% without losing the amorphous nature. It can be hypothesized that, due to the added timespan with increased molecular mobility during SC, the Flu-molecules were able to rearrange themselves in such a manner that Flu-Flu hydrogen bonds became dominant over Flu-PEtOx hydrogen bonds, unlike the electrospun ASDs where Flu-PEtOx hydrogen bonds remained dominant.

4. Conclusion

Even though Flu is proven to be a highly effective API against tropical diseases that are still affecting millions of people, sufficient bioavailability upon oral administration remains challenging due to the low solubility of the API and the limited physical stability of the currently applied formulations. In this work, solvent electrospinning was proven to be a highly promising alternative formulation technique using PEtOx as the excipient, as the produced nanofibrous Flu-PEtOx ASDs containing up to 55 wt% Flu showed a significant increase in solubility, hence bioavailability, in (acidic) aqueous media. Two important phenomena were considered to improve the physical stability

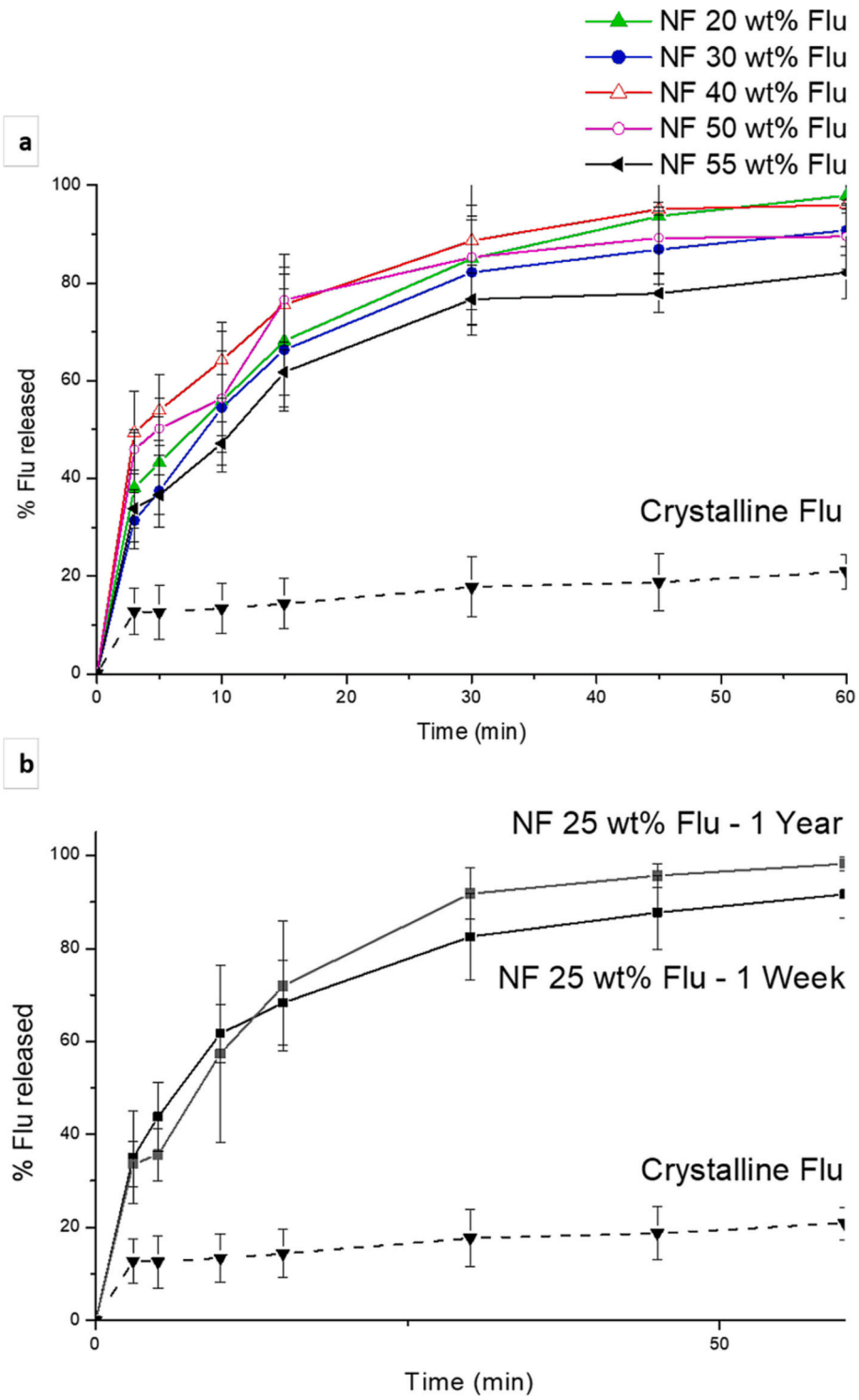

Fig. 5. (a) Dissolution profile of Flu-PEtOx ASDs *vs.* crystalline Flu, representing the cumulative release of Flu after one hour in a pH 1 dissolution medium. (b) A comparison of sink dissolution testing of a 25 wt% Flu-PEtOx ASD after one week *vs.* one year shows that no significant difference is found between the sink dissolution profiles of both ASDs. In the first hour full dissolution is already obtained, while crystalline Flu only reaches a 20% dissolution during the first hour.

of the formulations and, thereby, the efficacy of the drug delivery: the API-polymer interactions within the ASDs and the (long-term) amorphous nature of the ASDs. Together these correlated phenomena give an idea of both the thermodynamic and the kinetic stability of the ASD. Experimental ATR-FTIR analysis and computational molecular dynamics simulations supported the presence of strong, dominant and stable Flu-PEtOx hydrogen bond interactions, which enabled to significantly increase the Flu-loading in the ASDs up to 55 wt% by reducing the amount of PEtOx in the spinning solutions. It is hypothesized that, thanks to the rapid solvent evaporation during the electrospinning process, crystallization is inhibited as the dispersed Flu-molecules are quickly frozen into place and kinetically trapped within the PEtOx-matrix. Indeed, calculated self-diffusivity coefficients confirmed that the Flu-mobility within the ASDs was limited, as the coefficients were of the same order of magnitude as within a Flu-crystal. Additionally, XRD and MDSC analysis demonstrated the amorphous and single-phase

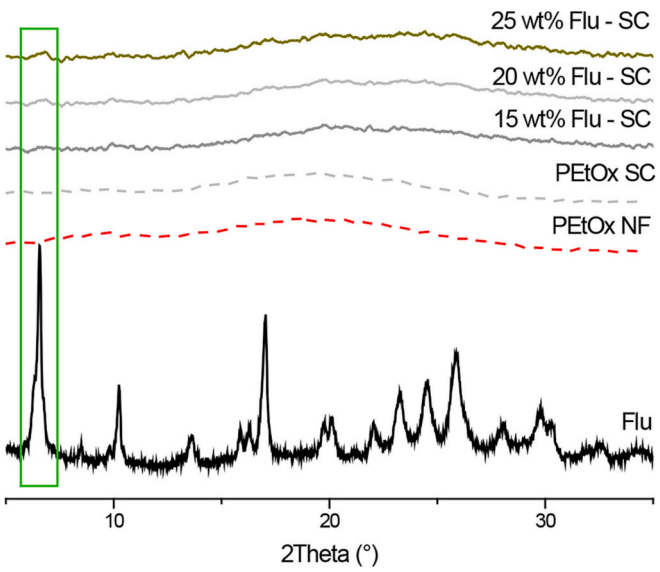

Fig. 6. XRD patterns of SC ASDs compared to the patterns of the pure components. From 15 wt% Flu-loadings onwards, a small Bragg peak at 6.5° becomes distinguishable. As proven by Fig. 4 (a), this peak is significant in indicating a higher ordening of the molecules leading up to a crystalline material. The SC technique can only guarantee complete amorphicity for low Flu-loadings.

nature of the Flu-PEtOx ASDs up to the high Flu-loadings of 55 wt%. As a consequence, Flu dissolution rates were quadrupled compared to crystalline Flu, and complete Flu release was achieved within one hour opposed to only 30% after five hours for crystalline Flu. The kinetic entrapment of amorphous Flu-molecules together with the Flu-PEtOx miscibility and the presence of strong and stable Flu-PEtOx hydrogen bond interactions led to the promising result that, even after two and a half years of storage, the nanofibrous Flu-PEtOx ASDs remained fully amorphous. Moreover, after storage for one year, a complete API-release within one hour could still be achieved. Based on these findings, it is clear that both the electrospinning technique and the excipient PEtOx provide several vital features for the formulation of high-loaded, time-stable ASDs with significantly improved drug-solubility, which is promising for the oral administration of not only Flu, but possibly also other BCS class II and IV APIs. This work further indicates that the strategy of combining experimental and computational work can add true value to obtain breakthroughs in the bioavailability improvement of future API-polymer ASD formulations. A new protocol was here established to simulate multi-scale Flu-PEtOx ASDs realistically, thereby providing a tool to thoroughly investigate and clarify the experimental observations and predict the characteristics of the real ASD. Indeed, such computational procedure allows to simulate possible API-polymer formulations and investigate the influence on ASD behavior under different experimental conditions, enabling to select which API-polymer formulations are promising to test experimentally. The expansion of this strategy will, therefore, be the subject of our future work, with the ultimate goal of developing a guide for drug selection and loading optimization for PEtOx-based electrospun ASDs.

Notes

The authors declare the following competing financial interest(s): JB, CV, RH and KDC are listed as inventors on a filed patent application covering high drug-loading ASD nanofibers as presented in this work. RH is one of the founders of Avroxa BV that commercializes poly(2-oxazoline)s as Ultroxa ®. The other authors declare no competing financial interest.

Author contributions

The manuscript was written through contributions of all authors. All authors have given approval to the final version of the manuscript.

CRediT authorship contribution statement

Jana Becelaere: Data curation, Formal analysis, Investigation, Methodology, Funding acquisition, Writing – original draft. **Elias Van Den Broeck:** Data curation, Formal analysis, Investigation, Methodology, Software, Writing – original draft. **Ella Schoolaert:** Writing – original draft, Writing – review & editing. **Valérie Vanhoorne:** Writing – review & editing. **Joachim F.R. Van Guyse:** Methodology, Writing – review & editing. **Maarten Vergaelen:** Conceptualization. **Sander Borgmans:** Formal analysis, Methodology, Software, Writing – review & editing. **Karolien Creemers:** Data curation, Formal analysis, Methodology. **Veronique Van Speybroeck:** Supervision, Funding acquisition, Writing – review & editing. **Chris Vervaet:** Conceptualization, Funding acquisition, Supervision, Writing – review & editing. **Richard Hoogenboom:** Conceptualization, Funding acquisition, Supervision, Writing – review & editing. **Karen De Clerck:** Conceptualization, Funding acquisition, Supervision, Writing – review & editing.

Acknowledgements

Financial support from the Research Foundation – Flanders (FWO) is gratefully acknowledged for funding the research through project grant G060518N and SB PhD grants 1S89118N of JB and 1S05517N of ES. Ghent University is also thanked by KDC, RH and CV for its continued support. The computational resources and services used were provided by Ghent University (Stevin Supercomputer Infrastructure), the VSC (Flemish Supercomputer Centre), funded by Ghent University, the Research Foundation - Flanders (FWO) and the Flemish Government. EVDB, SB. and VVS acknowledge the Research Foundation - Flanders (FWO) and the Research Fund of Ghent University (BOF).

Appendix A. Supplementary data

Supplementary data to this article can be found online at https://doi.org/10.1016/j.jconrel.2022.09.028.

References

[1] X. Xiong, M. Zhang, Q. Hou, P. Tang, Z. Suo, Y. Zhu, H. Li, Solid dispersions of telaprevir with improved solubility prepared by co-milling: formulation, physicochemical characterization, and cytotoxicity evaluation, Mater. Sci. Eng. C 105 (2019), 110012, https://doi.org/10.1016/j.msec.2019.110012.
[2] W. Wang, Z. Ye, H. Gao, D. Ouyang, Computational pharmaceutics - A new paradigm of drug delivery, J. Control. Release 338 (2021) 119–136, https://doi.org/10.1016/j.jconrel.2021.08.030.
[3] C. Brough, R.O. Williams, Amorphous solid dispersions and nano-crystal technologies for poorly water-soluble drug delivery, Int. J. Pharm. 453 (2013) 157–166, https://doi.org/10.1016/j.ijpharm.2013.05.061.
[4] M. Vialpando, S. Smulders, S. Bone, C. Jager, D. Vodak, M. Van Speybroeck, L. Verheyen, K. Backx, P. Boeykens, M.E. Brewster, J. Ceulemans, H.N. De Armas, K. Van Geel, E. Kesselaers, V. Hillewaert, S. Lachau-durand, G. Meurs, P. Psathas, B. Van Hove, G. Verreck, M. Voets, I. Weuts, C. Mackie, Evaluation of three amorphous drug delivery technologies to improve the oral absorption of flubendazole, J. Pharm. Sci. 105 (2016) 2782–2793, https://doi.org/10.1016/j.xphs.2016.03.003.
[5] M. O'Neill, C. Ballesteros, L. Tritten, E. Burkman, W.I. Zaky, J. Xia, A. Moorhead, S. A. Williams, T.G. Geary, Profiling the macrofilaricidal effects of flubendazole on adult female Brugia malayi using RNAseq, Int. J. Parasitol. Drugs Drug Resist. 6 (2016) 288–296, https://doi.org/10.1016/j.ijpddr.2016.09.005.
[6] M. O'Neill, J.F. Geary, D.W. Agnew, C.D. Mackenzie, T.G. Geary, Invitro flubendazole-induced damage to vital tissues in adult females of the filarial nematode Brugia malayi, Int. J. Parasitol. Drugs Drug Resist. 5 (2015) 135–140, https://doi.org/10.1016/j.ijpddr.2015.06.002.
[7] H.T. Sjoberg, N. Pionnier, G. Aljayyoussi, H.M. Metuge, A.J. Njouendou, V. C. Chunda, F.F. Fombad, D.B. Tayong, N.V.T. Gandjui, D.N. Akumtoh, P.W. N. Chounna, B.L. Ndzeshang, S. Lachaud, F. Tekle, L. Quirynen, M. Engelen, B. Baeten, A. Steven, S.A. Ward, M.J. Taylor, S. Wanji, J.D. Turner, Short-course, oral flubendazole does not mediate significant efficacy against Onchocerca adult

male worms or Brugia microfilariae in murine infection models, PLoS Negl. Trop. Dis. 13 (2019) 1–19, https://doi.org/10.1371/journal.pntd.0006356.
[8] M.P. Hübner, A. Ehrens, M. Koschel, B. Dubben, F. Lenz, S.J. Frohberger, S. Specht, L. Quirynen, S. Lachau-Durand, F. Tekle, B. Baeten, M. Engelen, C.D. Mackenzie, A. Hoerauf, Macrofilaricidal efficacy of single and repeated oral and subcutaneous doses of flubendazole in Litomosoides sigmodontis infected jirds, PLoS Negl. Trop. Dis. 13 (2019) 1–17, https://doi.org/10.1371/journal.pntd.0006320.
[9] G.L.B. de Araujo, F.F. Ferreira, C.E.S. Bernardes, J.A.P. Sato, O.M. Gil, D.L.A. de Faria, R. Loebenberg, S.R. Byrn, D.D.M. Ghisleni, N.A. Bou-Chacra, T.J.A. Pinto, S. G. Antonio, H.G. Ferraz, D. Zemlyanov, D.S. Gonçalves, M.E. Minas da Piedade, A new thermodynamically favored flubendazole/maleic acid binary crystal form: structure, energetics, and in silico PBPK model-based investigation, Cryst. Growth Des. (2018), https://doi.org/10.1021/acs.cgd.7b01807 acs.cgd.7b01807.
[10] L. Ceballos, C. Mackenzie, T. Geary, L. Alvarez, C. Lanusse, Exploring the potential of flubendazole in filariasis control: Evaluation of the systemic exposure for different pharmaceutical preparations, PLoS Negl. Trop. Dis. 8 (2014), e2838, https://doi.org/10.1371/journal.pntd.0002838.
[11] G.F. Chami, A.A. Kontoleon, E. Bulte, A. Fenwick, N.B. Kabatereine, E. M. Tukahebwa, D.W. Dunne, Diffusion of treatment in social networks and mass drug administration, Nat. Commun. 8 (2017) 1929, https://doi.org/10.1038/s41467-017-01499-z.
[12] A. Dominguez-Vazquez, H. Taylor, A.M. Ruvalcaba-Macias, R. Murphy, B. Greene, A.R. Rivas-Alcala, F. Beltran-Hernandez, Comparison of flubendazole and diethylcarbamazine in treatment of onchocerciasis, Lancet. 321 (1983) 139–143, https://doi.org/10.1016/S0140-6736(83)92753-8.
[13] M.M. Knopp, N. Chourak, F. Khan, J. Wendelboe, P. Langguth, T. Rades, R. Holm, Effect of polymer type and drug dose on the in vitro and in vivo behavior of amorphous solid dispersions, Eur. J. Pharm. Biopharm. 105 (2016) 106–114, https://doi.org/10.1016/j.ejpb.2016.05.017.
[14] G. Van Den Mooter, The use of amorphous solid dispersions: A formulation strategy to overcome poor solubility and dissolution rate, Drug Discov. Today Technol. 9 (2012) e79–e85, https://doi.org/10.1016/j.ddtec.2011.10.002.
[15] W.L. Chiou, S. Riegelman, Pharmaceutical applications of solid dispersion systems, J. Pharm. Sci. 60 (1971) 1281–1302, https://doi.org/10.1002/jps.2600600902.
[16] A. Smeets, R. Koekoekx, C. Clasen, G. Van den Mooter, Amorphous solid dispersions of darunavir: Comparison between spray drying and electrospraying, Eur. J. Pharm. Biopharm. 130 (2018) 96–107, https://doi.org/10.1016/j.ejpb.2018.06.021.
[17] S. Dedroog, C. Huygens, G. Van den Mooter, Chemically identical but physically different: A comparison of spray drying, hot melt extrusion and cryo-milling for the formulation of high drug loaded amorphous solid dispersions of naproxen, Eur. J. Pharm. Biopharm. 135 (2019) 1–12, https://doi.org/10.1016/j.ejpb.2018.12.002.
[18] A. Sahoo, N.S.K. Kumar, R. Suryanarayanan, Crosslinking: An avenue to develop stable amorphous solid dispersion with high drug loading and tailored physical stability, J. Control. Release 311–312 (2019) 212–224, https://doi.org/10.1016/j.jconrel.2019.09.007.
[19] P. Chakravarty, J.W. Lubach, J. Hau, K. Nagapudi, A rational approach towards development of amorphous solid dispersions: Experimental and computational techniques, Int. J. Pharm. 519 (2017) 44–57, https://doi.org/10.1016/j.ijpharm.2017.01.003.
[20] J. Pacułt, M. Rams-Baron, B. Chrząszcz, R. Jachowicz, M. Paluch, Effect of polymer chain length on the physical stability of amorphous drug-polymer blends at ambient pressure, Mol. Pharm. 15 (2018) 2807–2815, https://doi.org/10.1021/acs.molpharmaceut.8b00312.
[21] C. Persch, M.J. Müller, A. Yadav, J. Pries, N. Honné, P. Kerres, S. Wei, H. Tanaka, P. Fantini, E. Varesi, F. Pellizzer, M. Wuttig, The potential of chemical bonding to design crystallization and vitrification kinetics, Nat. Commun. 12 (2021) 4978, https://doi.org/10.1038/s41467-021-25258-3.
[22] L. Shang, Y. Yu, Y. Liu, Z. Chen, T. Kong, Y. Zhao, Spinning and applications of bioinspired fiber systems, ACS Nano 13 (2019) 2749–2772, https://doi.org/10.1021/acsnano.8b09651.
[23] K.S. Ogueri, C.T. Laurencin, Nanofiber technology for regenerative engineering, ACS Nano 14 (2020) 9347–9363, https://doi.org/10.1021/acsnano.0c03981.
[24] A. Luraghi, F. Peri, L. Moroni, Electrospinning for drug delivery applications: A review, J. Control. Release 334 (2021) 463–484, https://doi.org/10.1016/j.jconrel.2021.03.033.
[25] B. Démuth, A. Farkas, H. Pataki, A. Balogh, B. Szabó, E. Borbás, P.L. Sóti, T. Vigh, B. Kiserdei, J. Farkas, G. Mensch, I. Van Verreck, G. Assche, Z.K. Nagy Marosi, Detailed stability investigation of amorphous solid dispersions prepared by single-needle and high speed electrospinning, Int. J. Pharm. 498 (2016) 234–244, https://doi.org/10.1016/j.ijpharm.2015.12.029.
[26] Y. Ding, W. Li, F. Zhang, Z. Liu, N. Zanjanizadeh Ezazi, D. Liu, H.A. Santos, Electrospun fibrous architectures for drug delivery, tissue engineering and cancer therapy, Adv. Funct. Mater. 29 (2019) 1802852, https://doi.org/10.1002/adfm.201802852.
[27] D.G. Yu, J.J. Li, G.R. Williams, M. Zhao, Electrospun amorphous solid dispersions of poorly water-soluble drugs: A review, J. Control. Release 292 (2018) 91–110, https://doi.org/10.1016/j.jconrel.2018.08.016.
[28] D.G. Yu, J.M. Yang, C. Branford-White, P. Lu, L. Zhang, L.M. Zhu, Third generation solid dispersions of ferulic acid in electrospun composite nanofibers, Int. J. Pharm. 400 (2010) 158–164, https://doi.org/10.1016/j.ijpharm.2010.08.010.
[29] N. Bhardwaj, S.C. Kundu, Electrospinning: A fascinating fiber fabrication technique, Biotechnol. Adv. 28 (2010) 325–347, https://doi.org/10.1016/j.biotechadv.2010.01.004.
[30] A. Greiner, J.H. Wendorff, Electrospinning: A fascinating method for the preparation of ultrathin fibers, Angew. Chem. Int. Ed. 46 (2007) 5670–5703, https://doi.org/10.1002/anie.200604646.
[31] E. Schoolaert, I. Steyaert, G. Vancoillie, J. Geltmeyer, K. Lava, R. Hoogenboom, K. De Clerck, Blend electrospinning of dye-functionalized chitosan and poly (ϵ-caprolactone): Towards biocompatible pH-sensors, J. Mater. Chem. B 4 (2016) 4507–4516, https://doi.org/10.1039/c6tb00639f.
[32] B. Stubbe, Y. Li, M. Vergaelen, S. Van Vlierberghe, P. Dubruel, K. De Clerck, R. Hoogenboom, Aqueous electrospinning of poly(2-ethyl-2-oxazoline): Mapping the parameter space, Eur. Polym. J. 88 (2016) 1–9, https://doi.org/10.1016/j.eurpolymj.2016.09.014.
[33] L. Persano, A. Camposeo, C. Tekmen, D. Pisignano, Industrial upscaling of electrospinning and applications of polymer nanofibers: A review, Macromol. Mater. Eng. 298 (2013) 504–520, https://doi.org/10.1002/mame.201200290.
[34] H. Xu, F. Zhang, M. Wang, H. Lv, D.-G. Yu, X. Liu, H. Shen, Electrospun hierarchical structural films for effective wound healing, Biomater. Adv. 136 (2022), 212795, https://doi.org/10.1016/j.bioadv.2022.212795.
[35] D.G. Yu, M. Wang, R. Ge, Strategies for sustained drug release from electrospun multi-layer nanostructures, Wiley Interdiscip. Rev. Nanomed. Nanobiotechnol. (2021) 1–13, https://doi.org/10.1002/wnan.1772.
[36] S.F. Chou, D. Carson, K.A. Woodrow, Current strategies for sustaining drug release from electrospun nanofibers, J. Control. Release 220 (2015) 584–591, https://doi.org/10.1016/j.jconrel.2015.09.008.
[37] D. Liang, B.S. Hsiao, B. Chu, Functional electrospun nanofibrous scaffolds for biomedical applications, Adv. Drug Deliv. Rev. 59 (2007) 1392–1412, https://doi.org/10.1016/j.addr.2007.04.021.
[38] M.A. Mofazzal Jahromi, P. Sahandi Zangabad, S.M. Moosavi Basri, K. Sahandi Zangabad, A. Ghamarypour, A.R. Aref, M. Karimi, M.R. Hamblin, Nanomedicine and advanced technologies for burns: Preventing infection and facilitating wound healing, Adv. Drug Deliv. Rev. 123 (2018) 33–64, https://doi.org/10.1016/j.addr.2017.08.001.
[39] T. Vigh, B. Démuth, A. Balogh, D.L. Galata, I. Van Assche, C. Mackie, M. Vialpando, B. Van Hove, P. Psathas, E. Borbás, H. Pataki, P. Boeykens, G. Marosi, G. Verreck, Z.K. Nagy, Oral bioavailability enhancement of flubendazole by developing nanofibrous solid dosage forms, Drug Dev. Ind. Pharm. 9045 (2017) 1–8, https://doi.org/10.1080/03639045.2017.1298121.
[40] H. Liu, H. Wang, X. Lu, V. Murugadoss, M. Huang, H. Yang, F. Wan, D.G. Yu, Z. Guo, Electrospun structural nanohybrids combining three composites for fast helicide delivery, Adv. Compos. Hybrid Mater. (2022), https://doi.org/10.1007/s42114-022-00478-3.
[41] P.D. Nunes, J.F. Pinto, J. Henriques, A.M. Paiva, Insights into the release mechanisms of ITZ:HPMCAS amorphous solid dispersions: The role of drug-rich colloids, Mol. Pharm. 19 (2022) 51–66, https://doi.org/10.1021/acs.molpharmaceut.1c00578.
[42] G. Lemmens, J. Brouwers, J. Snoeys, P. Augustijns, T. Vanuytsel, Insight into the colonic disposition of celecoxib in humans, Eur. J. Pharm. Sci. 145 (2020), 105242, https://doi.org/10.1016/j.ejps.2020.105242.
[43] M. Davis, G. Walker, Recent strategies in spray drying for the enhanced bioavailability of poorly water-soluble drugs, J. Control. Release 269 (2018) 110–127, https://doi.org/10.1016/j.jconrel.2017.11.005.
[44] T. Xie, L.S. Taylor, Improved release of celecoxib from high drug loading amorphous solid dispersions formulated with polyacrylic acid and cellulose derivatives, Mol. Pharm. 13 (2016) 873–884, https://doi.org/10.1021/acs.molpharmaceut.5b00798.
[45] S. Saboo, N.A. Mugheirbi, D.Y. Zemlyanov, U.S. Kestur, L.S. Taylor, Congruent release of drug and polymer: A "sweet spot" in the dissolution of amorphous solid dispersions, J. Control. Release 298 (2019) 68–82, https://doi.org/10.1016/j.jconrel.2019.01.039.
[46] H. Fael, C. Ràfols, A.L. Demirel, Poly(2-Ethyl-2-Oxazoline) as an alternative to poly (Vinylpyrrolidone) in solid dispersions for solubility and dissolution rate enhancement of drugs, J. Pharm. Sci. 107 (2018) 2428–2438, https://doi.org/10.1016/j.xphs.2018.05.015.
[47] E. Boel, A. Smeets, M. Vergaelen, V.R. De la Rosa, R. Hoogenboom, G. Van den Mooter, Comparative study of the potential of poly(2-ethyl-2-oxazoline) as carrier in the formulation of amorphous solid dispersions of poorly soluble drugs, Eur. J. Pharm. Biopharm. 144 (2019) 79–90, https://doi.org/10.1016/j.ejpb.2019.09.005.
[48] S.P. Bhardwaj, K.K. Arora, E. Kwong, A. Templeton, S.D. Clas, R. Suryanarayanan, Mechanism of amorphous itraconazole stabilization in polymer solid dispersions: Role of molecular mobility, Mol. Pharm. 11 (2014) 4228–4237, https://doi.org/10.1021/mp5004515.
[49] V.R. De La Rosa, Poly(2-oxazoline)s as materials for biomedical applications, J. Mater. Sci. Mater. Med. (2014), https://doi.org/10.1007/s10856-013-5034-y.
[50] J.D. Friedl, V. Nele, G. De Rosa, A. Bernkop-Schnürch, Bioinert, stealth or interactive: How surface chemistry of nanocarriers determines their fate in vivo, Adv. Funct. Mater. 31 (2021) 2103347, https://doi.org/10.1002/adfm.202103347.
[51] R. Konradi, C. Acikgoz, M. Textor, Polyoxazolines for nonfouling surface coatings - A direct comparison to the gold standard PEG, Macromol. Rapid Commun. 33 (2012) 1663–1676, https://doi.org/10.1002/marc.201200422.
[52] S.E. Lapuk, L.S. Zubaidullina, M.A. Ziganshin, T.A. Mukhametzyanov, C. Schick, A. V. Gerasimov, Kinetic stability of amorphous solid dispersions with high content of the drug: A fast scanning calorimetry investigation, Int. J. Pharm. 562 (2019) 113–123, https://doi.org/10.1016/j.ijpharm.2019.03.039.
[53] T. Lorson, M.M. Lübtow, E. Wegener, M.S. Haider, S. Borova, D. Nahm, R. Jordan, M. Sokolski-Papkov, A.V. Kabanov, R. Luxenhofer, Poly(2-oxazoline)s based

biomaterials: A comprehensive and critical update, Biomaterials. 178 (2018) 204–280, https://doi.org/10.1016/j.biomaterials.2018.05.022.
[54] O. Sedlacek, B.D. Monnery, S.K. Filippov, R. Hoogenboom, M. Hruby, Poly(2-oxazoline)s - Are they more advantageous for biomedical applications than other polymers? Macromol. Rapid Commun. 33 (2012) 1648–1662, https://doi.org/10.1002/marc.201200453.
[55] I. Muljajew, S. Huschke, A. Ramoji, Z. Cseresnyés, S. Hoeppener, I. Nischang, W. Foo, J. Popp, M.T. Figge, C. Weber, M. Bauer, U.S. Schubert, A.T. Press, Stealth effect of short polyoxazolines in graft copolymers: Minor changes of backbone end group determine liver cell-type specificity, ACS Nano 15 (2021) 12298–12313, https://doi.org/10.1021/acsnano.1c04213.
[56] B.M. Chen, T.L. Cheng, S.R. Roffler, Polyethylene glycol immunogenicity: Theoretical, clinical, and practical aspects of anti-polyethylene glycol antibodies, ACS Nano (2021), https://doi.org/10.1021/acsnano.1c05922.
[57] R. Hoogenboom, Poly(2-oxazoline)s: A polymer class with numerous potential applications, Angew. Chem. Int. Ed. 48 (2009) 7978–7994, https://doi.org/10.1002/anie.200901607.
[58] R. Luxenhofer, G. Sahay, A. Schulz, D. Alakhova, T.K. Bronich, R. Jordan, A. V. Kabanov, Structure-property relationship in cytotoxicity and cell uptake of poly (2-oxazoline) amphiphiles, J. Control. Release 153 (2011) 73–82, https://doi.org/10.1016/j.jconrel.2011.04.010.
[59] B. Claeys, A. Vervaeck, C. Vervaet, J.P. Remon, R. Hoogenboom, B.G. De Geest, Poly (2-ethyl-2-oxazoline) as matrix excipient for drug formulation by hot melt extrusion and injection molding, Macromol. Rapid Commun. 33 (2012) 1701–1707, https://doi.org/10.1002/marc.201200332.
[60] B.D. Monnery, V.V. Jerca, O. Sedlacek, B. Verbraeken, R. Cavill, R. Hoogenboom, Defined high molar mass poly(2-Oxazoline)s, Angew. Chem. Int. Ed. 57 (2018) 15400–15404, https://doi.org/10.1002/anie.201807796.
[61] M. Vergaelen, B. Verbraeken, J.F.R. Van Guyse, A. Podevyn, A. Tigrine, V.R. de la Rosa, B.D. Monnery, R. Hoogenboom, Ethyl acetate as solvent for the synthesis of poly(2-ethyl-2-oxazoline), Green Chem. 22 (2020) 1747–1753, https://doi.org/10.1039/C9GC03872H.
[62] L. Buruaga, A. Gonzalez, J.J. Iruin, Electrospinning of poly (2-ethyl-2-oxazoline), J. Mater. Sci. 44 (2009) 3186–3191, https://doi.org/10.1007/s10853-009-3424-9.
[63] P. Chakravarty, J.W. Lubach, J. Hau, K. Nagapudi, A rational approach towards development of amorphous solid dispersions: Experimental and computational techniques, Int. J. Pharm. 519 (2017) 44–57, https://doi.org/10.1016/j.ijpharm.2017.01.003.
[64] K. Punčochová, J.Y.Y. Heng, J. Beránek, F. Štěpánek, Investigation of drug-polymer interaction in solid dispersions by vapour sorption methods, Int. J. Pharm. 469 (2014) 159–167, https://doi.org/10.1016/j.ijpharm.2014.04.048.
[65] N. Li, L.S. Taylor, Tailoring supersaturation from amorphous solid dispersions, J. Control. Release 279 (2018) 114–125, https://doi.org/10.1016/j.jconrel.2018.04.014.
[67] Sigma Aldrich, Safety Data Sheet Ultroxa®: Poly(2-ethyl-2-oxazoline), average Mn 50,000, PDI $\leq$ 1.25, 2018.
[68] R.J. Gowers, P. Carbone, A multiscale approach to model hydrogen bonding: The case of polyamide, J. Chem. Phys. 142 (2015), https://doi.org/10.1063/1.4922445.
[69] H. Chen, M. Li, Z. Lu, X. Wang, J. Yang, Z. Wang, F. Zhang, C. Gu, W. Zhang, Y. Sun, J. Sun, W. Zhu, X. Guo, Multistep nucleation and growth mechanisms of organic crystals from amorphous solid states, Nat. Commun. 10 (2019) 3872, https://doi.org/10.1038/s41467-019-11887-2.
[70] R.J. Young, P.A. Lovell, Introduction to Polymers, Third ed., CRC Press, 2011.
[71] F. Qian, J. Huang, Q. Zhu, R. Haddadin, J. Gawel, R. Garmise, M. Hussain, Is a distinctive single Tg a reliable indicator for the homogeneity of amorphous solid dispersion? Int. J. Pharm. 395 (2010) 232–235, https://doi.org/10.1016/j.ijpharm.2010.05.033.
[72] M. Gordon, J.S. Taylor, Ideal copolymers and the second-order transitions of synthetic rubbers. I. Noncrystalline copolymers, Rubber Chem. Technol. 26 (1953) 323–335, https://doi.org/10.5254/1.3539818.
[73] V.V. Jerca, F.A. Nicolescu, A. Baran, D.F. Anghel, D.S. Vasilescu, D.M. Vuluga, Synthesis and characterization of side-chain oxazoline–methyl methacrylate copolymers bearing azo-dye, React. Funct. Polym. 70 (2010) 827–835, https://doi.org/10.1016/j.reactfunctpolym.2010.07.018.
[74] J.A. Baird, L.S. Taylor, Evaluation of amorphous solid dispersion properties using thermal analysis techniques, Adv. Drug Deliv. Rev. 64 (2012) 396–421, https://doi.org/10.1016/j.addr.2011.07.009.
[75] J. Djuris, I. Nikolakakis, S. Ibric, Z. Djuric, K. Kachrimanis, Preparation of carbamazepine-Soluplus® solid dispersions by hot-melt extrusion, and prediction of drug-polymer miscibility by thermodynamic model fitting, Eur. J. Pharm. Biopharm. 84 (2013) 228–237, https://doi.org/10.1016/j.ejpb.2012.12.018.
[76] L.F.M. Franco, P.A. de Pessôa Filho, On the solubility of proteins as a function of pH: Mathematical development and application, Fluid Phase Equilib. 306 (2011) 242–250, https://doi.org/10.1016/j.fluid.2011.04.015.
[77] M. George, T.E. Abraham, Polyionic hydrocolloids for the intestinal delivery of protein drugs: Alginate and chitosan - a review, J. Control. Release 114 (2006) 1–14, https://doi.org/10.1016/j.jconrel.2006.04.017.
[78] V.P. Shah, Y. Tsong, P. Sathe, J.P. Liu, In vitro dissolution profile comparison–statistics and analysis of the similarity factor, f2, Pharm. Res. 15 (1998) 889–896, https://doi.org/10.1023/a:1011976615750.
[79] U. Paaver, J. Heinämäki, I. Laidmäe, A. Lust, J. Kozlova, E. Sillaste, K. Kirsimäe, P. Veski, K. Kogermann, Electrospun nano fi bers as a potential controlled-release solid dispersion system for poorly water-soluble drugs, Int. J. Pharm. 479 (2015) 252–260, https://doi.org/10.1016/j.ijpharm.2014.12.024.